15. Monari L, Chen SG, Brown P, et al. (1994) Fatal familial insomnia and familial Creutzfeldt-Jakob disease: different prion proteins determined by a DNA polymorphism. Proc Natl Acad Sci 91:2839–2842
16. Barbanti P, Fabbrini G, Salvatore M, et al. (1996) Polymorphism at codon 129 or 219 of PRNP and clinical heterogeneity in a previously unreported family with Gerstmann-Sträussler-Scherinker disease (PrP-P102L mutation). Neurology 47:734–741
17. Chapman J, Arlazoroff A, Goldfarb LG, et al. (1996) Fatal insomnia in a case of familial Creutzfeldt-Jakob disease with the codon 200^{Lys} mutation. Neurology 46:758–761
18. Young K, Clark HB, Piccardo P, Dlouhy SR, Ghetti B (1997) Gerstmann-Sträussler-Scherinker disease with the PRNP P102L mutation and valine at codon 129. Molecular Brain Research 44:147–150
19. Hainfellner JA, Parchi P, Kitamoto T, Jarius C, Gambetti P, Budka H (1999) A novel phenotype in familial Creutzfeldt-Jakob disease: Prion protein gene E200K mutation coupled with valine at codon 129 and type 2 protease-resistant prion protein. Ann Neurol 45:812–816
20. Yamada M, Itoh Y, Inaba A, et al. (1999) An inherited prion disease with a PrP P105L mutation: Clinicopathologic and PrP heterogeneity. Neurology 53: 181–188
21. Teratuto AL, Piccardo P, Reich EG, et al. (2002) Insomnia associated with thalamic involvement in E200K Creutzfeldt-Jakob disease. Neurology 58:362–267
22. Doh-ura K, Tateishi J, Sasaki H, Kitamoto T, Sasaki Y (1989) Pro-leu change at position 102 of prion protein is the most common but not the sole mutation related to Gerstmann-Sträussler syndrome. Biochem Biophys Res Commun 163:974–979
23. Furukawa H, Kitamoto T, Tanaka Y, Tateishi J (1995) New variant prion protein in a Japanese family with Gerstmann-Sträussler-Scherinker syndrome. Brain Res Mol Brain Res 30:385–388
24. Shibuya S, Higuchi J, Shin RW, Tateishi J, Kitamoto T (1998) Codon 219 Lys allele of PRNP is not found in sporadic Creutzfeldt-Jakob disease. Ann Neurol 43:826–828
25. Pocchiari M, Puopolo M, Croes EA, et al. (2004) Predictors of survival in sporadic Creutzfeldt-Jakob disease and other human transmissible spongiform encephalopathies. Brain 127: 2348–2359
26. Hill AF, Joiner S, Wadsworth JD, et al. (2003) Molecular classification of sporadic Creutzfeldt-Jakob disease. Brain 126:1333–1346
27. Satoh K, Muramoto T, Tanaka T, et al. (2003) Association of an 11–12 kDa protease-resistant prion protein fragment with subtypes of dura graft-associated Creutzfeldt-Jakob disease and other prion diseases. J General Virol 84:2885–2893
28. Kitamoto T, Shin RW, Doh-ura K, et al. (1992) Abnormal isoform of prion proteins accumulates in the synaptic structures of the central nervous system in patients with Creutzfeldt-Jakob disease. Am J Pathol 140:1285–1294
29. Young GS, Geschwind MD, Fischbein NJ, et al. (2005) Diffusion-weighted and fluid-attenuated inversion recovery imaging in Creutzfeldt-Jakob disease: High sensitivity and specificity for diagnosis. Am J Neuroradiol 26: 1551–1562
30. Hamaguchi T, Kitamoto T, Sato T, et al. (2005) Clinical diagnosis of MM2-type sporadic Creutzfeldt-Jakob disease. Neurology 64:643–648
31. Dagvadorj A, Peterson RB, Lee HS, et al. (2003) Spontaneous mutations in the prion protein gene causing transmissible spongiform encephalopathy. Ann Neurol 52:355–359
32. Mitrova E, Belay GI (2002) Creutzfeldt-Jakob disease with E200K mutation in Slovakia: characterization and development. Acta Virol 46:31–39
33. Taguchi Y, Mohri S, Ironside JW, Muramoto T, Kitamoto T (2003) Humanized knock-in mice expressing chimeric prion protein showed varied susceptibility to different human prions. Am J Pathol 163:2585–2593

Journal of Neuroscience Research 85:2196–2206 (2007)

Impairment of Microglial Responses to Facial Nerve Axotomy in Cathepsin S–Deficient Mice

Hai Peng Hao,[1] Katsumi Doh-ura,[2] and Hiroshi Nakanishi[1]*

[1]Laboratory of Oral Aging Science, Faculty of Dental Sciences, Kyushu University, Fukuoka, Japan
[2]Department of Prion Research, Tohoku University, Sendai, Japan

Cathepsin S (CS) is a lysosomal/endosomal cysteine protease especially expressed in cells of a mononuclear lineage including microglia. To better understand the role of CS in microglia, we investigated microglial responses after a facial nerve axotomy in CS-deficient (CS−/−) and wild-type mice. Microglia in both groups accumulated in the facial motor nucleus following axotomy. However, the mean number of microglia in CS−/− mice on the axotomized side was significantly smaller than that in wild-type mice. Microglia were found to adhere to injured motoneurons in wild-type mice, whereas microglia abutted on injured motoneurons without spreading on their surface in CS−/− mice. At the same time, the axotomy-induced down-regulation of tenasin-R, an antiadhesive perineuronal net for microglia, was partially abrogated in CS−/− mice. Primary cultured microglia prepared from CS−/− mice showed that CS deficiency caused significant suppression of migration and transmigration of microglia. In CS−/− mice, impaired recruitments of circulating monocytes and T lymphocytes and reduced expression of the class II major compatibility complex on the axotomized side were observed. Interestingly, cathepsin B, a typical lysosomal cysteine protease, was markedly expressed on the axotomized side in CS−/− but not in wild-type microglia. Finally, we compared axotomy-induced neuronal death in the two groups and found that the percentage of motoneurons that survived in CS−/− mice was significantly smaller than that in wild-type mice. The present study strongly suggests that CS plays a role in the migration and activation of microglia to protect facial motoneurons against axotomy-induced injury.

Key words: cathepsin S–deficient mice; facial nerve axotomy; microglia; cathepsin B; transmigration; motoneuron survival

Cathepsin S (CS) is a member of the lysosomal cysteine protease family, which is preferentially expressed in cells of mononuclear-phagocytic origin including microglia (Petanceska et al., 1996). In response to lipopolysaccharide (LPS), a substantial increase in the activity of CS secreted from both macrophages and microglia is observed (Petanceska et al., 1996). CS retains its proteolytic activity even after prolonged exposure to a neutral pH (Bromme et al., 1989, 1993). CS has been reported to degrade several extracellular matrix (ECM) molecules including fibrillar collagen, elasin, laminin, fibronectin, and heparan sulfate proteoglycans at a neutral pH (Liuzzo et al., 1999). CS-deficient (CS−/−) monocytic cells showed impaired subendothelial basement membrane transmigration (Sukhova et al., 2003). Furthermore, CS plays a pivotal role in antigen presentation because this enzyme is an essential requirement for invariant chain processing in antigen-presenting cells including dendritic cells and microglia (Nakagawa et al., 1999; Shi et al., 1999; Nishioku et al., 2002) without affecting expression of the class II major compatibility complex (MHC II). The cell type–specific localization and enzymatic nature of CS both contrast sharply with other types of lysosomal cysteine proteases including cathepsin B (CB). CB is expressed in almost all cell types and is also secreted from microglia as the heavy chain form in addition to the proform on stimulation with LPS (Ryan et al., 1995). However, it is well known that CB is irreversibly inactivated at a neutral pH. In addition to playing a role in intracellular proteolysis, CS secreted by microglia and monocytic cells may also play a role in extracellular proteolysis among different types of lysosomal cysteine proteases. We may therefore speculate that CS plays a specific role in the reactions of microglia and monocytic cells including migration, adhesion, transmigration, and antigen presentation (Nakanishi, 2003).

It is well known that microglia exhibit a series of reactions after facial nerve axotomy (Ravich et al., 1999; Moran and Graeber, 2004). Following axotomy, micro-

Contract grant sponsor: Ministry of Education, Science and Culture, Japan; Contract grant numbers: 17390495, 17659578, and 17659578 (all to H.N.).

*Correspondence to: Hiroshi Nakanishi, PhD, Laboratory of Oral Aging Science, Faculty of Dental Sciences, Kyushu University, Fukuoka 812-8582, Japan. E-mail: nakan@dent.kyushu-u.ac.jp

Received 1 November 2006; Revised 4 January 2007 and 24 February 2007; Accepted 8 March 2007

Published online 30 May 2007 in Wiley InterScience (www.interscience.wiley.com). DOI: 10.1002/jnr.21357

glia are rapidly activated and then are transformed into a deramified form; thereafter, they proliferate, adhere to injured motoneurons, and spread on their surfaces. Monocytic cells recruited to the brain parenchyma through the cerebral vasculature and the leptomeninges also adhere to injured motoneurons (Priller et al., 2001; Bechmann et al., 2005). Although the precise pathological significance of the perineuronal satellite position of microglia remains unclear, the adhesion of microglia to injured motoneurons may be essential for neuronal survival, thus leading to axonal regeneration. Activated microglia may displace synaptic input, a phenomenon known as synaptic stripping (Blinzinger and Kreutzberg, 1968). The tight adhesion of microglia could enhance uptake of diffusible molecules leaked from injured motoneurons and trans-synaptic uptake of their breakdown products as well as of pathogens (Ravich et al., 1999; Kalla et al., 2001). On the other hand, microglia express MHC II and costimulatory factors (Streit et al., 1989) and interact with T lymphocytes recruited to the axotomized facial motor nucleus (Ravich et al., 1998). Therefore, microglia may also play a pivotal role in immune surveillance as an antigen-presenting cells in the axotomized facial motor nucleus. Following a facial nerve axotomy, there was marked up-regulation in microglia of CS and cystatin C (CysC), the latter an endogenous inhibitor for cysteine proteases (Miyake et al., 1996; Uwabe et al., 1997). Up-regulation of CS may be closely associated with microglial responses to a facial nerve axotomy because ECM degradation is required for the rapid migration, adhesion, and transmigration of microglia and monocytic cells. Moreover, CS is essential for antigen presentation by microglia (Nishioku et al., 2002). However, no report has previously elucidated the precise function of CS in microglial reactions to a facial nerve axotomy.

In the present study, we examined the effects of CS deficiency on microglial reactions to a facial nerve axotomy and facial motoneuron survival. We found that CS deficiency markedly impaired cellular responses of microglia to a facial nerve axotomy, thereby promoting axotomy-induced facial motoneuron death.

MATERIALS AND METHODS

Animals

Heterozygous mice (CS+/−) mice on a DBA background were provided by Dr. William H. Brissette (Central Research Division, Pfizer Inc., Groton, CT; Nakagawa et al., 1999) and maintained under specific pathogen-free conditions at Kyushu University Faculty of Dentistry. Selection of CS−/− mice from littermates obtained by heterozygous coupling was performed by template genomic DNA isolated from tail biopsies examined to detect the neomycin cassette by neoexon 6– and exon 5–specific PCR with primers of cs6-1 (5′-TACCCGCTTCCATTGCTCAG-3′), cs6-2 (5′-TCTTTCAGGGCATCTTCGTC-3′), cs5-1 (5′-GGTTCTTGTGGTGCCTGTTG-3′), and cs5-2 (5′-GTGGCTTTGTAGGGATGGA-3′).

Surgical Procedures

All operations were performed under anesthesia with pentobarbital (40 mg/kg intraperitoneally, i.p.). The right facial nerves of 6-week-old CS−/− and wild-type mice were transected approximately 1 mm at the stylomastoid foramen. Failure of a mouse to move the whiskers on the right side of the face following recovery from anesthesia was considered verification of the success of the axotomy.

Immunohistochemistry

Detailed indirect fluorescent immunohistochemistry has been previously described (Nakanishi et al., 2001; Shimizu et al., 2005). Briefly, 2, 4, 7, 14, 30, and 50 days after axotomy, the specimens were obtained from CS−/− and wild-type mice (n = 4 each), which were anesthetized with sodium pentobarbital (40 mg/kg, i.p.) and killed by intracardiac perfusion with isotonic saline, followed by a chilled fixative consisting of 4% paraformaldehyde (PFA) in 0.2M phosphate-buffered saline (pH 7.4). After perfusion, the brain was removed, further fixed by immersion in the same fixative overnight at 4°C, and then immersed in 20% sucrose (pH 7.4) for 24 hr at 4°C. Floating parasagittal sections (30 μm thick) of the brain stem were prepared by a cryostat (CM1850 Leica, Nusloch, Germany) and stained with rabbit polyclonal anti-ionized calcium-binding adaptor molecule 1 (Iba1) antibody (1:500; Wako Pure Chemical Industries, Ltd., Osaka, Japan), OX6 (1:100; Serotec, Oxford, UK), mouse monoclonal anti–tenascin R (TNR) antibody (1:100; R&D Systems Inc., Minneapolis, MN), or rabbit polyclonal anti–choline acetyltransferase (ChAT, 1:500; Chemicon International) for 3 days at 4°C. After washing with phosphate-buffered saline (PBS), the sections were stained with biotinylated antirabbit, antimouse, or antigoat IgG (Vector Laboratories, Burlingame, CA) overnight. After washing with PBS, the sections were stained with ABC reagent (Vector Laboratories, Burlingame, CA) or Alexa 488 0.5% streptavidin (Molecular Probes, Eugene, OR). The sections that reacted with ABC reagent were developed with diaminobenzidine, dehydrated in alcohol and xylene, and then mounted. The sections that reacted with Alexa 488 streptavidin were mounted with Vectashield antifading medium (Vector Laboratories).

For double staining, floating parasagittal sections (30 μm thick) of the brain stem were incubated with goat polyclonal anti-CS antibody (1:300; Santa Cruz Biotechnology, Inc., Santa Cruz, CA), rabbit polyclonal anti-CB (1:200; Upstate, Lake Placid, NY), anti-ChAT (1:500), rabbit polyclonal anti-CysC (1:300; Upstate), or mouse monoclonal anti-CD3 (1:500; BD Biosciences, Bedford, MA) antibody for 3 days at 4°C. After washing with PBS, the sections were treated with 0.5% antirabbit or antigoat IgG conjugated with Cy3 (Jackson ImmunoResearch Laboratories, Inc., West Grove, PA) for 2 hr at room temperature. They were then further treated with anti-Iba1 antibody (1:500) or F4/80 (1:50; Serotec, Oxford, UK) for 3 days at 4°C. After washing with PBS, the sections were treated with 0.5% antirabbit IgG or antimouse IgG conjugated with Alexa 488 (Molecular Probes, Eugene, OR) for 2 hr at room temperature. The sections incubated with anti-ChAT antibody were also treated with 0.5% anti-

rabbit IgG conjugated with Alexa 488 (Molecular Probes) for 2 hr at room temperature. The sections were treated with mouse monoclonal anti-GFAP antibody (Sigma, St. Louis, MO) for 3 days at 4°C and then were further incubated with 0.5% antimouse IgG conjugated with Cy3 (Jackson Immunoresearch Laboratories). The sections were mounted in the Vectashield antifading medium (Vector Laboratories, Burlingame, CA) and examined by a confocal laser scanning microscope (CLSM; LSM510META, Carl Zeiss, Jena, Germany).

Evaluation of Microglial Morphology

To quantitatively describe the differences in microglial morphology between CS−/− and wild-type mice after axotomy, we adopted a transformation index (TI), which was calculated by the equation, [perimeter of cell (μM)]^2/4π [cell area (μm^2)] (Fujita et al., 1996). Five sections (30 μm thick) stained with anti-Iba1 antibody were randomly selected from each of the CS−/− and wild-type mice (n = 3 each). Images of individual sections, photographed with a conventional CCD camera with a 20× objective (numerical aperture = 0.75), were analyzed with an image analyzer to determine their perimeters and areas. The TI was calculated for the axotomized and control sides of the CS−/− and wild-type mice 2, 4, and 7 days after axotomy.

Electrophoresis and Immunoblotting

The supernatant fractions of the facial nuclei were prepared from CS−/− (n = 3) and wild-type (n = 3) mice 7 days after axotomy, in which the mice were anesthetized with sodium pentobarbital (40 mg/kg, i.p.) and killed by intracardiac perfusion with isotonic saline. Each homogenate was electrophoresed in 7%–12% sodium dodecyl sulfate (SDS)–polyacrylamide gels. Proteins on SDS gels were transferred electrophoretically to nitrocellulose membranes. The protein transfers were blocked in 5% skim milk for 1 hr at room temperature under gentle agitation. The blots were then incubated with anti-CS (1:1,000), anti-CB (1:1,000), anti-CysC (1:1,000), anti-TNR (1:500), or antiactin (1:1,000, Santa Cruz Biotechnology, Santa Cruz, Santa Cruz, CA) antibodies overnight at 4°C under gentle agitation. After washing, the blots were incubated with 0.02% horseradish peroxidase (HRP)–labeled donkey antirabbit or antimouse IgG (Amersham). Subsequently, the membrane-bound, HRP-labeled antibodies were detected by an enhanced chemiluminescence detection system (ECL kit, Amersham) with an image analyzer LAS-1000 (Fuji Photo Film, Tokyo, Japan). The protein bands were then scanned and analyzed densitometrically.

mRNA Extraction and Reverse Transcriptase (RT)-PCR

mRNA was prepared from the facial nuclei from CS−/− (n = 3) and wild-type (n = 3) mice 7 days after axotomy, and then the mice were anesthetized with sodium pentobarbital (40 mg/kg, i.p.) using a QuickPrep micro mRNA purification kit (Amersham Oharmacia Biotech, England, UK), and the first cDNA was synthesized using SuperScript II (Invitrogen, Carlsbad, CA). For PCR, the cDNA was amplified by Tag DNA polymerase (Invitrogen). Reverse transcription was performed at 60°C for 15 min in 0.5 mg of mRNA. PCR amplification was performed in the DNA amplifier cycle (Techne Duxford, UK) after an initial cycle at 94°C for 2 min for 40 cycles of 1 min at 94°C and 1.5 min at 60°C. The RT-PCR products were run on 2% agarose gel and stained with ethidium bromide. Glyceroldehydes-3-phosphate dehydrogenase (GAPDH)–specific primers were used as a control with 1 mL of template cDNA. Primers for CS were 5′-GACATTGCCTGACACTGTGG-3′ and 5′-CATGTTCACATTGCCCGTA-3′, primers for CB were 5′-CTCTGGAGCATGGAGCTTCT-3′ and 5′-ATGCCACAGTGGTTTTCTCC-3′, primers for CysC were 5′-AGCGAGTACAAC-AAGGGCAG-3′ and 5′-CAAGAAGAGTGAAGCCAGGG-3′, and primers for GAPDH were 5′-TCCACCACCCTGTTGCTGTA-3′ and 5′-ACCACAGTCCATGCCATCAC-3′.

Microglial Culture

Microglia were isolated from mixed primary cell cultures from whole-brain samples of 3-day-old CS−/− and wild-type mice according to methods described previously (Nishioku et al., 2002). Eagle's minimal essential medium (MEM) containing 10% fetal calf serum, penicillin G (40 U/mL), and streptomycin (50 mg/mL) was used for culture medium. After 10–14 days in culture, floating cells and weakly attached cells in the mixed glial cell layer were isolated by shaking of the flask. The resulting cell suspension was transferred to a petri dish (Falcon 1001, Lincoln Park, NJ) and allowed to adhere at 37°C. Unattached cells were removed after 30 min, and microglia were isolated as strongly adhering cells. The microglia were more than 96% pure, as determined by the immunostaining of Iba1.

Cell Proliferation Assay

Cell viability was measured 24 hr after treatment with macrophage colony-stimulating factor (M-CSF, R&D Systems Inc., Minneapolis, MN) or granulocyte macrophage colony-stimulating factor (GM-CSF, Genzyme, Cambridge, MA) by WST-8 conversion to water-soluble formazan by mitochondrial dehydrogenase (Cell Counting Kit-8, Dojindo, Kumamoto, Japan). Briefly, WST-8 was added to the culture medium of primary cultured microglia prepared from CS−/− and wild-type mice growing in serum-free medium and incubated at 37°C for 4 hr. The supernatant was transferred to 96-well dishes and then was quantitated using a plate reader at 450 nm.

Cell Migration Assay

Cell migration of microglia was assessed using the Boyden chamber. Polycarbonate filters with pores of 3 μM precoated with fibronectin (Becton Dickison Labware, Bedford, MA) were used. Five hundred microliters of microglial cell suspension in serum-free MEM containing 0.3% bovine serum albumin prepared from CS−/− and wild-type mice was plated on cell inserts at a cell density of 10^5. All inserts were dipped into lower wells contained 750 μL of serum-free MEM containing 100 μM ATP as a chemical attractant. The plates were incubated at 37°C in a 10% CO_2 atmosphere for 6 and 24 hr. Cells remaining on the upper surface of the

membrane were removed by wiping, and migrated cells were fixed with 4% PFA and subjected to Diff-Quik stain (Sysmex Corp., Kobe, Japan). Microglia that migrated to the lower surface of the membrane were manually counted in eight randomly chosen fields under a microscope with a 20× objective. Each assay was performed in triplicate.

Cell Transmigration Assay

Cell transmigration of microglia was assessed using a Matrigel chamber. Polycarbonate filters with pores of 8 μM precoated with Matrigel basement membrane matrix (BD Biosciences) were used. Five hundred microliters of microglial cell suspension in serum-free MEM containing 0.3% bovine serum albumin prepared from CS−/− and wild-type mice was plated on cell inserts at a cell density of 2×10^5. All inserts were dipped into lower wells contained 750 μL of serum-free MEM containing 100 μM ATP as a chemical attractant. In some experiments using primary culture microglia prepared from wild-type mice, benzyloxycarbonyl-Phe-Leu-α-keto-β-aldehyde (Z-FL-COCHO; Calbiochem, San Diego, CA), a specific inhibitor of CS, was added to serum-free MEM. Plates were incubated at 37°C in 10% CO_2 atmosphere for 24 hr. Cells remaining on the upper surface of the membrane were removed by wiping and the transmigrated cells were fixed with 4% PFA and subjected to Diff-Quik stain (Sysmex Corp.). The number of microglia that transmigrated to the lower surface of the membrane was manually counted in eight randomly chosen fields under a microscope with a 20× objective. Each assay was performed in triplicate.

Intrasplenic Injection of 6-Carboxylfluorescein Diacetate (CFDA)

CS−/− and wild-type mice (n = 3 each) were anesthetized with sodium pentobarbital (40 mg/kg, i.p.). A 0.5 cm incision was made on the left lateral abdomen. After preparing the surface of the spleen, 100 μL of a solution containing 2% of the long-lasting fluorescent tracker CFDA (Molecular Probes) in 0.1M PB was slowly injected. Twenty-four hours after the intrasplenic injection of CFDA, the right-side facial nerves were axotomized.

Quantitative Analysis of Facial Motoneurons

The optical dissector method using CLSM images (Jinno et al., 1998; Shimizu et al., 2005) was used to measure the numerical density of facial motoneurons. Five 30-μm-thick serial sections of a facial motor nucleus stained with anti-ChAT antibody were prepared from CS−/− and wild-type mice (n = 3 each) that had been subjected to facial nerve axotomy 4, 7, 30, and 50 days earlier. Images of individual sections were taken as a stack at 1-μm step size along the z direction with a 20× objective by a CLSM (LSM510MET). Data were transferred to a Power Mac G4 computer (Apple) and then analyzed using NIH Image software (version 1.62). Antibodies from the surface sufficiently permeated the full thickness of both CS−/− and wild-type mice brain sections. The number of ChAT-immunoreactive cells in each of five serial sections of a facial motor nucleus was summed. The data were averaged for each animal and then for each group. The calculated numerical profile densities of the groups were compared using the Student t test.

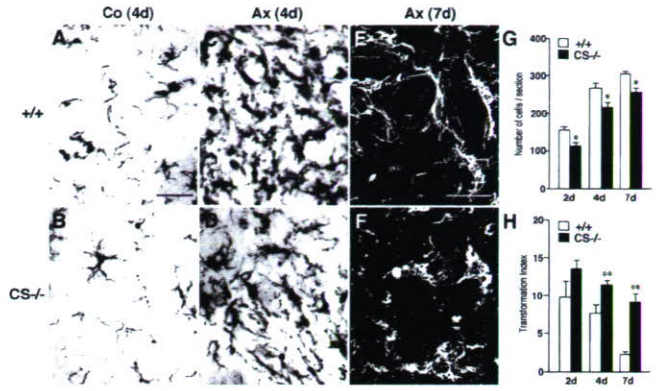

Fig. 1. Microglial responses following facial nerve axotomy in CS−/− and wild-type mice. **A:** Iba1-stained microglia in facial motor nuclei on control side (Co) of wild-type mice 4 days after axotomy. Scale bar = 50 μm. **B:** Iba1-stained microglia in facial motor nuclei on Co side of CS−/− mice 4 days after axotomy. **C:** Iba1-stained microglia in facial motor nuclei on axotomized side (Ax) of wild-type mice 4 days after axotomy. **D:** Iba1-stained microglia in facial motor nuclei on Ax side of CS−/− mice 4 days after axotomy. **E:** High-resolution CLSM images of Iba1-stained microglia on the axotomized side of facial motor nuclei of wild-type mice 7 days after axotomy. Scale bar = 25 μm. **F:** High-resolution CLSM images of Iba1-stained microglia on the axotomized side of facial motor nuclei of CS−/− mice 7 days after axotomy. Each section was taken as a stack at 1-μm step size along the z direction with a 100× objective by a CLSM. **G:** Number of microglia accumulated in axotomized facial motor nuclei of wild-type and CS−/− mice (open and solid columns, respectively) 2, 4, and 7 days after axotomy. Each column and bar represents the mean ± SD of three experiments (*significant difference at $P < 0.05$). **H:** TI of microglia accumulated in the axotomized facial motor nuclei of wild-type and CS−/− mice (open and solid columns, respectively) 2, 4, and 7 days after axotomy. TI was calculated by the equation [perimeter of cell (μM)]^2 /4π [cell area (μm^2)].

Statistical Analysis

Data are expressed as means ± SDs. The statistical analyses were performed using the Student t test.

RESULTS

Alterations of Microglial Responses to Facial Nerve Axotomy in CS−/− Mice

No obvious abnormality in CS−/− mice compared to wild-type mice was noticed. We first focused on the microglial responses to the facial nerve axotomy. Following axotomy, microglia on the axotomized side of mice in both groups showed activated cell morphology characterized by a large cell body with thick processes. On the other hand, microglia on the control side maintained a normal ramified morphology (Fig. 1A,B). Four days after axotomy, there was a marked difference between the two groups in the morphology of microglia on the axotomized side. In wild-type mice, microglia had relatively small

cell bodies with thin processes (Fig. 1C). In contrast, in CS−/− mice most microglia still had rather large cell bodies with short processes (Fig. 1D). These morphological differences in microglia became more prominent 7 days after axotomy. CLSM images clearly showed that microglia spread on the surfaces of injured motoneurons, forming a thin continuum rimlike structure, in the wild-type mice (Fig. 1E). In CS−/− mice, most microglia still had rather large cell bodies with short processes and abutted injured motoneurons without spreading on their surface (Fig. 1F).

We further quantitated the number and morphological transformation of microglia on the axotomized side of the facial motor nuclei of both groups. As shown in Figure 1G, the mean number of microglia that had accumulated on the axotomized side of the facial motor nuclei of CS−/− mice was significantly smaller than that of wild-type mice. The morphological transformation of microglia after axotomy was also quantitated as a TI using the equation [perimeter of cell (μM)]^2/4π [cell area (μm^2)]. The mean TI of CS−/− mice was significantly larger than that of wild-type mice 4 days after axotomy (Fig. 1H).

Reduced TNR Down-Regulation in Facial Motor Nuclei of CS−/− Mice following Axotomy

Next, we tried to determine why the CS−/− microglia failed to spread on the surfaces of facial motoneurons after axotomy. It has been reported that TNR that presents in the perineuronal net of motoneurons acts as antiadhesive for activated microglia (Angelov et al., 1998). Furthermore, expression of TNR was markedly down-regulated after axotomy. Therefore, it is tempting to speculate that insufficient down-regulation of TNR in CS−/− mice may prevent microglia from spreading onto the surfaces of axotomized facial motoneurons. To determine if this were true, we examined the level of TNR in the facial motor nuclei of CS−/− and wild-type mice after axotomy. In both groups, the total amount of TNR significantly decreased on the axotomized side (Fig. 2A). However, there was a greater decrease in the amount of TNR in the CS−/− mice than in the wild-type mice. This was substantiated with immunostaining with anti-TNR antibody (Fig. 2B). Although the immunoreactivity for TNR diffusely spread throughout a facial motor nucleus, the most intense immunoreactivity was found on the surface of cell somata of motoneurons in both groups. Seven days after axotomy, there was a marked reduction in the immunoreactivity for TNR on the axotomized side of the facial motor nuclei of wild-type mice. In contrast, only a moderate reduction in immunoreactivity for TNR was found in the CS−/− mice.

Effects of CS Deficiency on ATP-Induced Migration/Transmigration and GM-CSF-Induced Proliferation of Primary Cultured Microglia

Rapid accumulation of microglia occurred in the facial nuclei after axotomy mainly because of the proliferation and migration of microglia as a result of cellular activation (Ravich et al., 1999; Moran and Graeber, 2004). There is increasing evidence that in addition to the contributions made by proliferation and migration, recruitment of monocytic cells through the cerebral vasculature and the leptomeninges also adds to the increased number of microglia on the axotomized side of the facial motor nucleus (Priller et al., 2001; Bechmann et al., 2005). Thus, we next compared the proliferative, migratory, and proliferative abilities of primary cultured microglia prepared from CS−/− and wild-type mice because there was a significant reduction in the number of microglia on the axotomized side of the facial motor nuclei of CS−/− mice.

M-CSF is a major mitogen for microglia in the axotomized facial nucleus (Raivichet al., 1994). Furthermore, an experiment involving GM-CSF binding in axotomized facial nuclei showed GM-CSF to be a plausible mitogen (Ravich et al., 1991). We thus used both M-SCF and GM-CSF as mitogens to examine the effect of CS deficiency on cell-proliferating ability. As shown in Figure 3A, there was no significant difference between the two groups in the cell-proliferating ability of microglia after stimulation with either M-CSF or GM-CSF. We next conducted ATP-induced cell migration assay using a Boyden chamber. The wild-type and CS−/− microglia that migrated to the opposite side of the fibronectin-coated membrane after treatment with ATP were counted. As shown in Figure 3B, the mean number of migrated CS−/− microglia 24 hr after treatment with

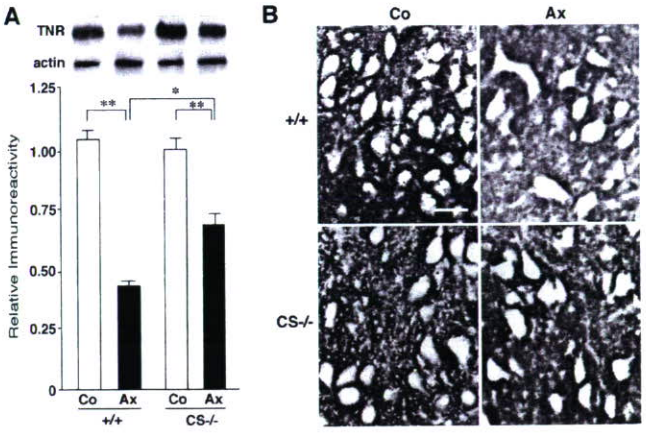

Fig. 2. Reduction in axotomy-induced down-regulation of TNR in facial motor nuclei of CS−/− mice 7 days after axotomy. **A:** Immunoblot analyses of TNR levels on the control (Co) and axotomized (Ax) sides (open and solid columns, respectively) of facial motor nuclei of CS−/− and wild-type mice. Mean relative immunoreactivity of TNR band was determined using expression of actin as an internal control. Each column and bar represents the mean ± SD of three experiments (**significant difference at $P < 0.01$). **B:** Immunohistochemical staining of TNR on Co and Ax sides of facial motor nuclei of CS−/− and wild-type mice. A marked reduction in the immunoreactivity for TNR was observed in axotomized facial motor nuclei of wild-type mice but not in CS−/− mice. Scale bar = 75 μm.

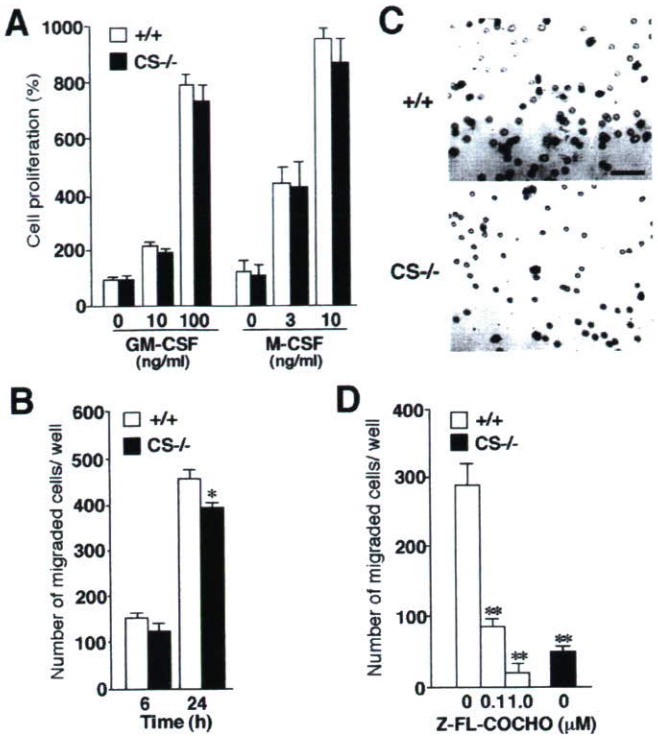

Fig. 3. Effects of CS deficiency on proliferation, migration, and transmigration of primary cultured microglia. **A:** Mean survival ratio of CS−/− and wild-type microglia 24 hr after treatment with M-CSF or GM-CSF. Each column and bar represents the mean ± SD of three experiments. **B:** ATP-induced migration of primary cultured microglia prepared from CS−/− and wild-type mice detected by the Boyden chamber. Mean number of CS−/− and wild-type microglia that migrated to the opposite side of a fibronectin-coated membrane, assessed by a Boyden chamber 6 and 24 hr after treatment with ATP (100 μM). Each column and bar represents the mean ± SD of three experiments (*significantly different from the wild-type microglia at $P < 0.05$). **C, D:** ATP-induced transmigration of primary cultured microglia prepared from CS−/− and wild-type mice, detected by a Matrigel invasion chamber. **C:** CS−/− and wild-type microglia that transmigrated to the opposite side of the Matrigel basement membrane matrix. Scale bar = 85 μm. **D:** Mean number of CS−/− and wild-type microglia as well as wild-type microglia treated with Z-FL-COCHO that transmigrated to opposite side of the Matrigel basement membrane matrix 24 hr after treatment with ATP (100 μM). Each column and bar represents the mean ± SD of three experiments (**significantly different from the wild-type control at $P < 0.01$).

ATP (100 μM) was slightly but significantly smaller than that of migrated wild-type microglia. We further conducted an ATP-induced cell transmigration assay using a Matrigel invasion chamber. The mean number of CS−/− microglia transmigrated through the Matrigel basement membrane matrix 24 hr after treatment with ATP (100 μM) was significantly lower than that of wild-type microglia (Fig. 2C,D). Furthermore, a specific inhibitor of CS, Z-FL-COCHO, significantly inhibited the transmigration of wild-type microglia through the Matrigel basement membrane matrix in a dose-dependent manner (Fig. 3D).

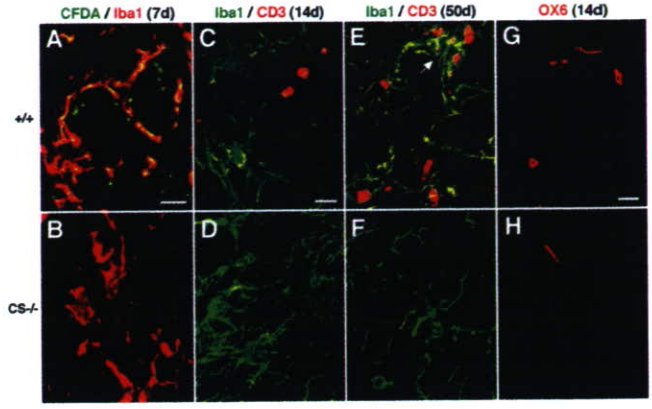

Fig. 4. Impairment of axotomy-induced recruitment of CFDA-labeled splenocytes and T lymphocytes in the facial motor nuclei of CS−/− mice. **A:** Immunofluorescent CLSM image of facial motor nuclei of wild-type mice 7 days after axotomy showing that the CFDA-labeled cells (green) are visible on the axotomized side. Scale bar = 35 μ. **B:** Immunofluorescent CLSM image of facial motor nuclei of CS−/− mice 7 days after axotomy showing that the CFDA-labeled cells (green) are not visible on the axotomized side. The CFDA-labeled cells corresponded well with microglia (red), which spread on the surface of injured facial motoneurons. **C:** CLSM image of infiltrated CD3-positive T lymphocytes (red) and Iba1-positive microglia (green) in facial motor nuclei of wild-type mice 14 days after axotomy. Scale bar = 40 μm. **D:** CLSM image of infiltrated CD3-positive T lymphocytes (red) and Iba1-positive microglia (green) in facial motor nuclei of CS−/− mice 14 days after axotomy. **E:** CLSM image of infiltrated CD3-positive T lymphocytes (red) and Iba1-positive microglia (green) in facial motor nuclei of wild-type mice 50 days after axotomy. Scale bar = 40 μm. **F:** CLSM image of infiltrated CD3-positive T lymphocytes (red) and Iba1-positive microglia (green) in facial motor nuclei of CS−/− mice 50 days after axotomy. **G:** CLSM images of immunoreactivity for MHC II-positive cells in facial motor nuclei of wild-type mice 14 days after axotomy. Scale bar = 30 μm. **H:** CLSM images of immunoreactivity for MHC II-positive cells in facial motor nuclei of CS−/− mice 14 days after axotomy.

Z-FL-COCHO did not have a significant cytotoxic effect on primary cultured microglia in the concentration range used in this study (data not shown).

Impaired Recruitment of Monocytic Cells and T Lymphocytes and Reduced MHC II Expression in Facial Motor Nuclei of CS−/− Mice after Axotomy

To further evaluate the effects of CS deficiency on cell transmigration, we examined the recruitment of monocytic cells and T lymphocytes into facial motor nuclei after axotomy. Seven days after axotomy, CFDA-fluorescent granules were detected on the axotomized side of the facial motor nuclei of intrasplenic CFDA-injected wild-type mice. These CFDA fluorescent granules were found to localize in 13% ± 3% of the Iba1-positive microglia (Fig. 4A). In contrast, we could not detect any CFDA fluorescent granules in the facial motor nuclei of CFDA-injected CS−/− mice (Fig. 4B). These obser-

vations indicated that approximately 10% of the Iba1-positive cells that accumulated on the axotomized side thus originated from circulating monocytic cells and that the CS deficiency significantly suppressed the recruitment of these monocytic cells.

We also examined recruitment of T lymphocytes in the facial motor nuclei 14 and 50 days after axotomy. In wild-type mice, CD3-positive T lymphocytes were detected to infiltrate the axotomized side (Fig. 4C,E). The mean number of CD3-positive cells per section 14 and 50 days after axotomy was approximately 4 and 12 cells/section, respectively. Fifty days after axotomy, the aggregated microglia were frequently surrounded by infiltrated CD3-positive T lymphocytes (Fig. 3E, arrow). In contrast, no CD3-positive cells were detected in the facial motor nuclei following axotomy (Fig. 4D,F).

We next examined the expression of MHC II because interactions with T lymphocytes are required for the induction of MHC II in antigen-presenting cells. As shown in Figure 4G, immunoreactivity for MHC II was observed in microglia-like cells as well as in perivascular-like cells in the facial motor nuclei of wild-type mice 14 days after axotomy. In contrast, only MHC II–positive perivascular-like cells were observed on the axotomized side of CS−/− mice (Fig. 4H).

Differential Axotomy-Induced Changes in CS, CB, and CysC Levels in CS−/− and Wild-Type Mice

We next measured the levels of CS, CB, and CysC, an endogenous cysteine protease inhibitor, at both the mRNA and protein levels in the facial motor nuclei of mice from both groups after axotomy. In wild-type mice, the mean levels of CS mRNA and CS protein (28-kDa active form) in the facial motor nucleus significantly increased after axotomy (Fig. 5A,B,E). Immunoblot analysis showed that under reducing conditions, using a CB-specific antibody, there were two mature forms of CB: a 29-kDa single-chain species and a 26-kDa heavy-chain species. Mean levels of CB mRNA and CB protein (29-kDa single-chain form) the facial motor nuclei of wild-type mice were not significantly changed after axotomy, whereas those of CS−/− mice significantly increased after axotomy (Fig. 5A,C,F). In contrast, mean levels of CysC mRNA and CysC protein (14 kDa) in the facial motor nuclei of CS−/− mice were significantly smaller than those of wild-type mice. After axotomy, mean levels of CysC mRNA and CysC protein (14 kDa) in the facial motor nuclei of mice in both groups significantly increased (Fig. 5A,D,G).

Localization of CS, CB, and CysC in the Facial Motor Nucleus after Facial Nerve Transection

Indirect immunofluorescent staining was used to further elucidate how cellular localization of CS, CB, and CysC increased after axotomy. It was found that CS localized in activated microglia that spread on the surfaces of injured motoneurons in wild-type mice (Fig. 6A). In contrast, immunoreactivity for CS was barely detectable in

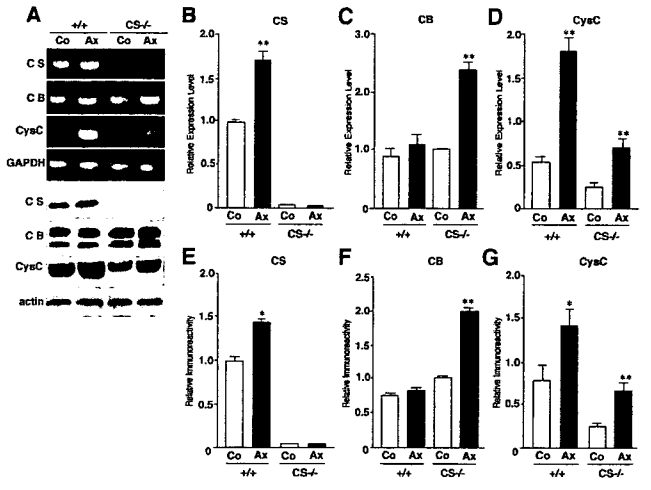

Fig. 5. Changes in CS, CB, and CysC levels in facial motor nuclei of CS−/− and wild-type mice 7 days after axotomy. **A:** Immunoblot and RT-PCR analyses of CS, CB, and CysC on control (Co) and axotomized (Ax) sides of facial motor nuclei of CS−/− and wild-type mice. **B:** Mean relative mRNA expression of CS, determined using expression of GAPDH as an internal control, on Co and Ax sides (open and solid columns, respectively) of facial motor nuclei of CS−/− and wild-type mice. **C:** Mean relative mRNA expression of CB, determined using expression of GAPDH as an internal control, on Co and Ax sides (open and solid columns, respectively) of facial motor nuclei of CS−/− and wild-type mice. **D:** Mean relative mRNA expression of CysC, determined using expression of GAPDH as an internal control, on Co and Ax sides (open and solid columns, respectively) of facial motor nuclei of CS−/− and wild-type mice. Each column and bar represents the mean ± SD of three experiments (**significantly different from the value in Co at $P < 0.01$). **E:** Mean level of CS protein, determined using expression of actin as an internal control, on Co and Ax sides (open and solid columns, respectively) of facial motor nuclei of CS−/− and wild-type mice. **F:** Mean level of CB protein, determined using expression of actin as an internal control, on Co and Ax sides (open and solid columns, respectively) of facial motor nuclei of CS−/− and wild-type mice. **G:** Mean level of CysC protein, determined using expression of actin as an internal control, on Co and Ax sides (open and solid columns, respectively) of facial motor nuclei of CS−/− and wild-type mice. Each column and bar represents the mean ± SD of three experiments (*$P < 0.05$ versus value in Co, **$P < 0.01$ versus value in Co).

the axotomized facial motor nuclei of CS−/− mice (Fig. 6B). In contrast, intense immunoreactivity for CB was observed in the facial motoneurons but not in the perineuronal microglia of wild-type mice (Fig. 6C). Interestingly, the immunoreactivity for CB markedly increased in activated microglia abutting injured motoneurons in CS−/− mice (Fig. 6D). In contrast, immunoreactivity for CysC increased in activated microglia on the axotomized side of facial motor nuclei from both groups (Fig. 6E,F).

Decrease in Facial Motoneuron Survival following Axotomy in CS−/− Mice

Finally, we examined the effects of CS deficiency on axotomy-induced facial motoneuron death. On days

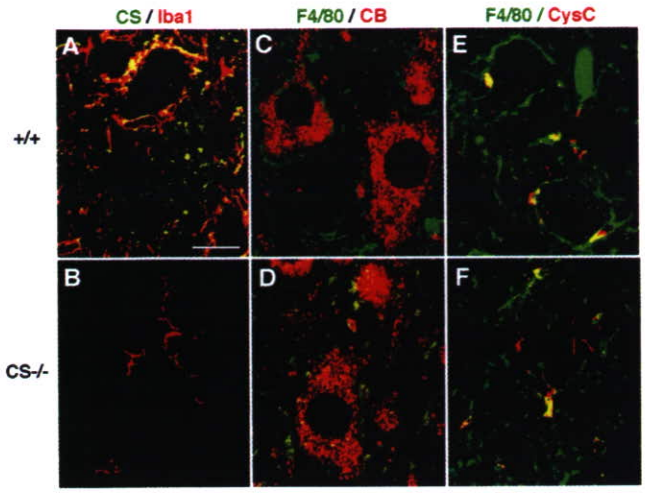

Fig. 6. Localization of CS, CB, and CysC in activated microglia that adhered to injured facial motoneurons 7 days after axotomy. **A:** Immunofluorescent CLSM image of CS (green). Scale bar = 25 μm. **B:** Immunofluorescent CLSM image of Iba1 (red). **C:** CLSM image of F4/80 (green). **D:** CLSM image of CB (red). Immunoreactivity to CB was observed in microglia abutting the facial motoneurons of CS−/− mice but not in the perineuronal microglia of wild-type mice. **E:** CLSM image of F4/80 (green). **F:** CLSM image of CysC (red). Immunoreactivity to CysC was observed in microglia of both groups.

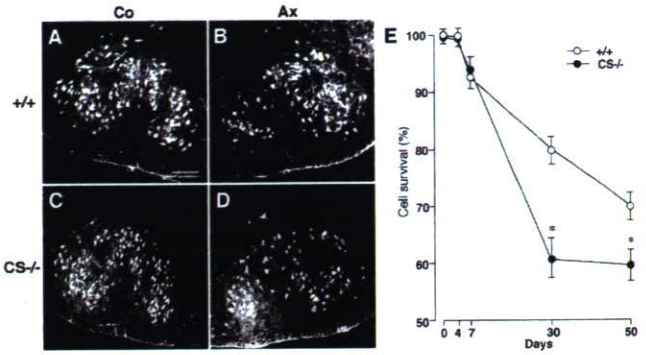

Fig. 7. Decrease in facial motoneuron survival following axotomy in CS−/− mice. **A:** Immunofluorescent CLSM image of ChAT-positive facial motoneurons on control (Co) side of wild-type mice. Scale bar = 150 μm. **B:** Immunofluorescent CLSM image of ChAT-positive facial motoneurons on axotomized (Ax) side of wild-type mice. **C:** Immunofluorescent CLSM image of ChAT-positive facial motoneurons on Co side of CS−/− mice. **D:** Immunofluorescent CLSM image of ChAT-positive facial motoneurons on Ax side of CS−/− mice. **E:** Mean cell survival ratio of ChAT-positive facial motoneurons 4, 7, 30, and 50 days after axotomy in CS−/− and wild-type mice. Each column and bar represents the mean ± SD of four experiments (*significant difference between the 2 groups at $P < 0.05$). Five serial sections (30 μm thick) stained with anti-ChAT antibody were prepared from each group. CLSM images of ChAT-positive facial motoneurons in each section were taken as a stack at 1-μm step size along the z direction with a 20× objective. The number of ChAT-immunoreactive cells in the facial motor nucleus of each section was determined, and the values of all the serial sections of an entire facial motor nucleus were summed.

4, 7, 30, and 50 after axotomy, we counted the ChAT-positive facial motoneurons on both the control and axotomized sides of the facial motor nuclei from the mice in both groups. As shown in Figure 7, the difference between the two groups was statistically significant ($P < 0.05$) 30 and 50 days after axotomy. The mean percentage of ChAT-positive facial motoneurons that survived in wild-type mice 30 days after axotomy was 79.9% ± 2.3% (2,123 ± 65 cells on the control side, 1,697 ± 42 cells on the axotomized side), and the mean percentage that survived 50 days after axotomy was 69.7% ± 2.2% (2,204 ± 61 cells on the control side, 1,536 ± 44 cells on the axotomized side). The mean percentage of ChAT-positive facial motoneurons in CS−/− mice 30 days after axotomy was 60.7% ± 3.3% (1,917 ± 46 cells on the control side, 1,164 ± 39 cells on the axotomized side), and the mean percentage that survived 50 days after axotomy was 59.7% ± 2.6% (2,315 ± 43 cells on the control side, 1,382 ± 50 cells on the axotomized side).

DISCUSSION

Impairment of Migration and Transmigration of Activated Microglia and Monocytic Cells in CS−/− Mice

Following axotomy, microglia can become activated and therefore come into direct contact with injured motoneurons and begin to proliferate without turning into phagocytes (Ravich et al., 1999; Moran and Graeber, 2004). There is increasing evidence that the recruitment of monocytic cells through the cerebral vasculature and the leptomeninges also contributes to the increased number of microglia (Priller et al., 2001; Bechmann et al., 2005). In the present study, we found that cellular responses of microglia to facial nerve axotomy were markedly impaired in CS−/− mice. The mean number of activated microglia that accumulated on the axotomized side of facial motor nuclei of CS−/− mice was significantly smaller than that on the axotomized side of facial motor nuclei of wild-type mice. Furthermore, the activated microglia the accumulated on the axotomized side of facial motor nuclei of CS−/− mice exhibited some characteristics similar to those of phagocytic cells.

These observations show that the expression profiles of CB and CysC on the axotomized side of facial nuclei of CS−/− mice were quite different from those of wild-type mice. After axotomy, CB increased as the mature forms of activated microglia accumulated in the facial motor nuclei of CS−/− mice, but not in wild-type mice. CysC also significantly increased in activated microglia accumulated in the facial motor nuclei of both groups following axotomy. However, the expression of CysC on both sides of the facial motor nuclei of CS−/− mice was significantly smaller than that in wild-type mice. CB is known to increase in stimulated peripheral macrophages and phagocytic microglia in the CNS. More recently, CB has been demonstrated to be a major neurotoxic molecule released from activated microglia (Kingham and Pocock,

2001; Gan et al., 2004). Although the increased CB in activated microglia of CS−/− mice could compensate for some roles of CS, it may endow them with both phagocytic and neurotoxic capabilities.

In the present study, intrasplenic injection of CFDA and the invasion assay showed that the recruitment and transmigratory abilities of monocytic cells of CS−/− mice were significantly impaired. These results are consistent with the finding that CS degrades major components of the basement membrane of the cerebral vasculature and the leptomeninges including type IV and type V collagens, fibronectin, laminin, vitronectin, and heparan sulfate proteoglycans (Rao et al., 2003). CS has been reported to degrade ECM macromolecules in the brain parenchyma and basement membrane such as proteoglycans, laminin, collagens, elastin, and chondroitin sulfate proteoglycan, even at a neutral pH (Petanceska et al., 1996; Liuzzo et al., 1999). Thus, the impaired migration and recruitment of microglia/monocytic cells are considered mainly responsible for the significant reduction in the mean number of activated microglia accumulated on the axotomized side of the facial motor nuclei of CS−/− mice.

Impairment of Axotomy-Induced Microglial Spreading on Surfaces of Axotomized Facial Motoneurons in CS−/− Mice

There was a marked difference between two groups in the morphology of activated microglia that adhered to injured facial motoneurons. In wild-type mice, activated microglia spread on the surfaces of injured motoneurons. In contrast, CS−/− microglia failed to spread on injured motoneurons and stayed with the relatively large cell bodies. CS deficiency can reasonably be considered responsible for the different morphological changes in activated microglia in CS−/− mice after axotomy because CS can degrade molecules that influence the adhesion properties of microglia.

Perineuronal nets, typically consisting of a chondroitin sulfate proteoglycan complex with hyaluronan and tenascin glycoprotein, are the most conspicuous feature of a specialized neuronal microenvironment. Angelov et al. (1998) reported that TNR in the perineuronal net of motoneurons becomes down-regulated after a peripheral-nerve axotomy. They further showed TNR to be an antiadhesive for microglia. Thus, down-regulation of TNR may make axotomized motoneurons accessible to the stable adhesion of activated microglia, leading to their spreading on the neuronal surface. More recently, a quantitative analysis of vibrissal movement revealed that TNR deficiency promoted functional recovery after a facial nerve axotomy (Guntinas-Lichius et al., 2005). It is likely that down-regulation of TNR and the subsequent adhesion of activated microglia on neuronal surfaces are therefore necessary for the survival and axonal regeneration of axotomized facial motoneurons. In the present study, the amount of TNR in the facial nuclei of CS−/− mice 7 days after axotomy was significantly larger than that in wild-type mice. Axotomy-induced down-regulation of TNR can result from proteolytic degradation by CS secreted from activated microglia. Therefore, insufficient degradation of TNR can reasonably be considered to prevent microglia from spreading on the surfaces of injured motoneurons in CS−/− mice. Additional experiments are needed to further clarify the proteolytic profiles of CS to TNR and other perineuronal nets.

Increase in Axotomy-Induced Motoneuron Death in CS−/− Mice

The rate of neuronal death after a peripheral-nerve axotomy varies significantly between species. In adult rats, the rate of motoneuron death after axotomy is very low, whereas in adult mice, it is relatively high (Ravich et al., 1998; Kiryu-Seo et al., 2005). DBA mice were used in the present study, which showed that a deficiency of CS significantly decreased motoneuron viability in late post-axotomy stages. There are two possible reasons for this decreased neuronal viability in CS−/− mice after axotomy.

One possible explanation is that there is impaired microglial response to axotomy, as CS is known to be exclusively expressed in cells with a monocytic lineage, which include microglia but not neurons. However, there is increasing evidence that microglia do not affect neuronal survival and axonal regeneration. In mouse models deficient in interleukin-6 or macrophage colony-stimulating factor, there was a reduction in the number of microglia during the early response to facial nerve axotomy, but this did not influence the degeneration of facial motoneurons (Galiano et al., 2001; Kalla et al., 2001). To ablate the proliferating microglia, Gowing et al. (2006) recently generated transgenic mice that express a mutant form of herpes simplex virus type 1 thymidine kinase driven by the myeloid-specific CD11b promoter. They showed that specific ablation of proliferating microglia in these transgenic mice could be achieved by the administration of ganciclovir. Using this system, they found that the elimination of proliferating microglia after axotomy did not influence the degeneration of motoneurons after a hypoglossal nerve axotomy.

In contrast, T lymphocytes have been reported to infiltrate into the facial motor nucleus during the early response to a facial nerve axotomy (Galiano et al., 2001; Kalla et al., 2001). Furthermore, the recruited T lymphocytes have been demonstrated to prevent axotomy-induced motoneuron death (Serpe et al., 1999; Byram et al., 2004). Through interactions with T lymphocytes, antigen-presenting cells including microglia are cross-activated. In the present study, we could detect infiltrated CD3-positive T lymphocytes in the facial motor nuclei of wild-type mice but not in those of CS−/− mice following axotomy. CS may also play a role in recruitment of T lymphocytes to the brain parenchyma.

We have previously reported that microglia used CS for the degradation of the invariant chain (Ii) into class II-associated Ii peptide (CLIP; Nishioku et al., 2002; Naka-

nishi, 2003). CS deficiency can reasonably be considered to prevent removal of CLIP from the antigen-binding cleft of MHC II, thus inhibiting antigen presentation to $CD4^+$ T lymphocytes. The expression of MHC II markedly decreased on the axotomized side of the facial motor nuclei of CS−/− mice. Therefore, defective interactions with T lymphocytes may account for the reduced expression of MHC in CS−/− mice after axotomy. However, it was reported that MHC II–positive cells were almost completely limited to perivascular macrophages in a facial axotomy model (Liu et al., 2005). Additional experiments are necessary to elucidate the contribution of defective interaction with T lymphocytes to impaired microglial responses in CS−/− mice after axotomy.

ACKNOWLEDGMENT

We thank Dr. Sandra Ferry (Kyushu University) for providing us with valuable advice in conducting this study.

REFERENCES

Angelov DN, Walther M, Streppel M, Guntinas-Lichius O, Neiss WF, Probstmeier R, Pesheva P. 1998. Tenascin-R is antiadhesive for activated microglia that induce downregulatiuon of the protein after peripheral nerve injury: a new role in neuronal protection. J Neurosci 18:6218–6229.

Bechmann I, Goldmann J, Kovac AD, Kwidzinski E, Simburger E, Naftolin F, Dirnagl U, Nitsch R, Priller J. 2005. Circulating monocytic cells infiltrate layers of anterograde axonal degeneration where they transform into microglia. FASEB J 19:647–649.

Blinzinger K, Kreutzberg GW. 1968. Displacement of synaptic terminals from regenerating motoneurons by microglial cells. Z Zellforsch 85:145–157.

Bromme D, Bonneau PR, Lachance P, Wiederanders B, Krischke H, Peters C, Thomas DY, Storer AC, Vernet T. 1993. Functional expression of human cathepsin S in Saccharomyces cerevisiae. Purification and characterization of the recombinant enzyme. J Biol Chem 268: 4832–4838.

Bromme D, Steinert A, Friebe S, Fittkau S, Wiederanders B, Kirschke H, 1989. The specificity of bovine spleen cathepsin S. Biochem J 264:475–481.

Byram SC, Carson MJ, DeBoy CA, Serpe CJ, Sanders VM, Jones KJ. 2004. CD4-positive T cell-mediated neuroprotection requires dual compartment antigen presentation. J Neurosci 24:4333–4339.

Fujita H, Tanaka J, Toku K, Tateishi N, Suzuki Y, Matsuda S, Sakanaka M, Maeda N. 1996. Effects of GM-CSF and ordinary supplements on the ramification of microglia in culture: a morphological study. Glia 18:269–281.

Galiano M, Liu ZQ, Kalla R, Bohatschek M, Koppius A, Gschwendtner A, Xu S, Werner A, Kloss CUA, Jones LL, Bluethmann H, Raivich G. 2001. Interleukin-6 (IL6) and cellular responses to facial nerve injury: effects on lymphocyte recuitment, early microglial activation and axonal outgrowth in IL6-deficient mice. Eur J Neurosci 14:327–341.

Gan L, Ye S, Chu A, Anton K, Yi S, Vincent VA, von Schack D, Chin D, Murray J, Lohr S, Pattyhy L, Gonzalez-Zulueta M, Nikolich K, Urfer R. 2004. Identification of cathepsin B as a mediator of neuronal death induced by Aβ-activated microglial cells using a functional genomics approach. J Biol Chem 279:205565–205572.

Gowing G, Vallières L, Julien JP. 2006. Mouse model for ablation of proliferating microglia in acute CNS injuries. Glia 53:331–337.

Guntinas-Lichius O, Angelov DN, Morellini F, Lenzen M, Skouras E, Schachner M, Irintchev A. 2005. Opposite impact of tenascin-C and tenascin-R deficiency in mice on the functional outcome of facial nerve repair. Eur J Neurosci 22:2171–2179.

Jinno S, Aika Y, Fukuda T, Kosaka T. 1998. Quantitative analysis of GABAergic neurons in the mouse hippocampus, with optical dissector using confocal laser scanning microscope. Brain Res 814:33–70.

Kalla R, Liu Z, Xu S, Koppius A, Imai Y, Kloss CUA, Kohsaka S, Gschwendtner A, Moller JS, Werner A, Raivich G. 2001. Microglia and early phase of immune surveillance in the axotomized facial motor nucleus: impaired microglial activation and lymphocyte recruitment but no effect on neuronal survival or axonal regeneration in macrophage-colony stimulating factor-deficient mice. J Comp Neurol 436:182–201.

Kingham PJ, Pocock JM. 2001. Microglial secreted cathepsin B induces neuronal apoptosis. J Neurochem 76:1475–1484.

Kiryu-Seo S, Hirayama T, Kato R, Kiyama H. 2005. Noxa is a critical mediator of p53-dependent motor neuron death after nerve injury in adult mouse. J Neurosci 25:1442–1447.

Liu ZQ, Bohatschek M, Pfeffer K, Bluethmann H, Raivich G. 2005. Major histocompatibility complex (MHC2+) perivascular macrophages in the axotomized facial motor nucleus are regulated by receptors for interferon-γ (IFNγ) and tumor necrosis factor (TNF). Neuroscience 131:283–292.

Liuzzo JP, Petanceska S, Moscatelli D, Devi LA. 1999. Inflammatory mediators regulate cathepsin S in macrophages and microglia: a role in attenuating heparan sulfate interactions. Mol Med 5:320–333.

Miyake T, Gahara Y, Nakayama M, Yamada H, Uewabe K, Kitamura T. 1996. Up-regulation of cystatin C by microglia in the rat facial nucleus following axotomy. Mol Brain Res 37:273–282.

Moran LM, Graeber MB. 2004. The facial nerve axotomy model. Brain Res Rev 44:154–178.

Nakanishi H. 2003. Microglial functions and proteases. Mol Neurobiol 27:163–176.

Nakanishi H, Zhang J, Koike M, Nishioku T, Okamoto Y, Kominami E, von Figura K, Peters C, Yamamoto K, Saftig P, Uchiyama Y. 2001. Involvement of nitric oxide released from microglia/macrophages in pathological changes of cathepsin D-deficient mice. J Neurosci 21:7526–7533.

Nakagawa TY, Brissette WH, Lira PD, Griffiths RJ, Petrushova N, Stock J, McNeish JD, Eastmen SE, Howard ED, Clarke SRM, Rosloniec EF, Elliott EA, Rudensky AY. 1999. Impaired invariant chain degradation and antigen presentation and diminished collagen-induced arthritis in cathepsin S null mice. Immunity 19:207–217.

Nishioku T, Hashimoto K, Yamashita K, Liou SY, Kagamiishi Y, Maegawa H, Katsube N, Peters C, von Figura K, Saftig P, Katunuma N, Yamamoto K, Nakanishi H. 2002. Involvement of cathepsin E in exogenous antigen processing in primary cultured murine microglia. J Biol Chem 277:4816–4822.

Petancesk S, Canoll P, Devi LA. 1996. Expression of rat cathepsin S in phagocytic cells. J Biol Chem 271:4403–4409.

Priller J, Flügel A, Wehner T, Boenter M, Hass CA, Prinz M, Fernández-Klett F, Prass K, Bechmann I, de Boer BA, Frotscher M, Kreutzbrg GW, Persons D, Dirnagl U. 2001. Targeting gene-modified hematopoietic cells to the central nervous system: use of green fluorescent protein uncovers microglial engraftment. Nat Med 7:356–1361.

Rao JS. 2003. Molecular mechanisms of glioma invasiveness: the role of proteases. Nat Rev Cancer 3:489–501.

Ravich G, Bohatschek M, Kloss CUA, Werner A, Jones LL, Kreutzberg GW. 1999. Neuroglial activation repertoire in the injured brain: graded response, molecular mechanisms and cues to physiological function. Brain Res Rev 30:77–105.

Raivich G., Gehrmann J, Kreutzberg GW. 1991. Increase of macrophage colony-stimulating factor and granulocyte-macrophage colony-stimulating factor receptors in the regenerating rat facial nucleus. J Neurosci Res 30:682–686.

Ravich G, Jone LL, Kloss CUA, Werner A, Neumann H, Kreutzberg GW. 1998. Immune surveillance in the injured nervous system: T-lymphocytes invade the axotomized mouse facial motor nucleus and aggregate around sites of neuronal degeneration. J Neurosci 18:5804–5816.

Raivich G., Moreno-Flores MT, Moller JC, Kreutzberg GW. 1994. Inhibition of posttraumatic microglial proliferation in a genetic model of macrophage colony-stimulating factor deficiency in the mouse. Eur J Neurosci 6:1615–1618.

Ryan RE, Solane BF, Sameni M, Wood PL. 1995. Microglial cathepsin B: an immunological examination of cellular and secreted species. J Neurochem 65:1035–1045.

Serpe CJ, Kohm AP, Huppenbauer CB, Sanders VM, Jones KJ. 1999. Exacerbation of facial motoneuron loss after facial nerve transction in severe combined immunodeficient (scid) mice. J Neurosci 19:RC7.

Shi GP, Villadangos JA, Dranoff G, Small C, Gu L, Haley KJ, Riese R, Ploegh HL, Chapman HA, 1999. Cathepsin S required for normal MHC class II peptide loading and germinal center development. Immunity 10:197–206.

Shimizu, Hayashi Y, Yamasaki R, Yamada J, Zhang J, Ukai K, Koike M, Mine K, von Figura K, Peters C, Saftig P, Fukuda T, Uchiyama Y, Nakanishi H. 2005. Proteolytic degradation of glutamate decarboxylase mediates disinhibition of hippocampal CA3 pyramidal cells in cathepsin D-deficient mice. J Neurochem 94:680–690.

Streit WJ, Graeber MB, Kreutzberg GW. 1989. Peripheral nerve lesion produces increased levels of major histocompatibility complex antigens in the central nervous system. J Neuroimmunol 21:117–123.

Sukhova GK, Zhang Y, Pan JH, Wada Y, Yamamoto T, Naito M, Kodama T, Tsimikas S, Witztum JL, Lu ML, Sakara Y, Chin MT, Libby P, Shi GP. 2003. Deficiency of cathepsin S reduces atherosclerosis in LDL receptor-deficient mice. J Clin Invest 111:897–906.

Uwabe K, Gahara Y, Yamada H, Miyake T, Kitamura T. 1997. Identification and characterization of a novel gene (neurorep 1) expressed in nerve cells and up-regulated after axotomy. Neuroscience 80:501–509.

日本臨牀　66巻 増刊号1（2008年1月28日発行）別刷

アルツハイマー病

—基礎研究から予防・治療の新しいパラダイム—

III. 臨　床　編

アルツハイマー病の診断

新しい診断法の開発

アミロイド画像化用プローブ

工藤幸司　　古本祥三　　岡村信行

III. 臨 床 編

アルツハイマー病の診断
新しい診断法の開発

アミロイド画像化用プローブ

The probes for amyloid imaging

工藤幸司[1]　古本祥三[1]　岡村信行[2]

Key Words：アルツハイマー病，アミロイドイメージングプローブ，タウイメージングプローブ，近赤外線蛍光プローブ

はじめに

アミロイド画像化(イメージング)用プローブは，アルツハイマー病(AD)の代表的病理像の一つ，老人斑の主構成成分であるアミロイドβ蛋白(Aβ)のβシート構造に高い親和性を有する標識ないしは非標識化合物であり，画像としてのアミロイドイメージングを可能にするために用いられる．

AD診断におけるアミロイドイメージングの有用性については本誌岡村らおよび樋口らの別稿に譲るとして，本稿ではpositron emission tomography(PET)プローブを中心に，アミロイドイメージングに用いられる種々のプローブ群の現状，開発状況，薬理学的特性などにつき概説するとともに，併せてタウイメージング用PETプローブのそれらについても若干言及してみたい．

1. アミロイドイメージング用プローブに求められる一般的な特性および特徴

いずれのアミロイドイメージング用プローブもまず第1にβシート構造をとったAβに対して高い親和性をもつことが必要である．プローブは化学構造的にCongo redタイプ，thioflavin Tタイプおよびそのほかに大きく分類される．普通のレセプターアッセイでは多少の標識リガンドの構造の違いは克服できるが，例えばCongo redタイプ標識リガンドのAβバインディングは同タイプのプローブによってよく置換されるが，その他のタイプのそれらによっては極めて置換されにくく，またその逆も真であることが知られている[1,2]．このことはプローブの基本構造の違いによってAβバインディングサイトはそれぞれ異なること，いいかえればプローブの基本構造の違いの数だけバインディングサイトが存在することを示唆している．

Aβ はAD患者脳内に蓄積する．当然プローブは血液-脳関門を透過することが必要であるが，投与直後には急速かつ大用量が脳へ移行し，その後急速に脳からウォッシュアウトされるという極めて相反する2つの特性をもたせなければならないことが，これらプローブの開発を難しくしている最大の要因である．

現状のアミロイドイメージングはプローブのいずれかの部位に標識された同位体を追跡することから，代謝された同位体が標的以外に集積するような標識法は避けなければならない．[^{18}F]標識体において脱フッ素により^{18}Fイオンが骨に集積し，あたかも(頭蓋)骨PET画像とな

[1]Yukitsuka Kudo, Shozo Furumoto: Biomedical Engineering Research Organization (TUBERO), Tohoku University 東北大学先進医工学研究機構　[2]Nobuyuki Okamura: Department of Pharmacology, Tohoku University School of Medicine　東北大学大学院医学系研究科 機能薬理学分野

0047-1852/08/¥40/頁/JCLS

ることはよく経験することである[3]．プローブごとに適切な標識法および部位を開発しなくてはならないことも，プローブ開発を難しくしている一因である．

2. アミロイドイメージング用PETプローブ

Aβに親和性が高く，しかも血液-脳関門を容易に透過する化合物を標識し，ADの診断に応用しようとするアイデアは1990年代初めのころから提唱されていたが，具体例として我々の目に触れたのはこの分野のパイオニア，ピッツバーグ大学Klunkらのプロトタイププローブchrysamine-G[4]が最初である(**図1**)．彼らのchrysamine-G系統プローブはX-34，更にmethoxy-X04へと引き継がれている．X-34が更に修飾されたのがペンシルベニア大Kung夫妻らによって報告されたBSB，ISB，IMSBであり，夫妻らは更にTZDM，TZPI，IBOXをも報告している(**図1**)．著者らのプローブはBF-108から始まり，次いでBF-168へと研究が転換した(**図1**)．

これら以外にも数多くのプローブが学術誌および学会で報告されてきたが，それらの集大成が**図2**に示した臨床研究に供されたプローブ群である．2002年初頭，世界で初めてAD患者にアミロイドイメージング用PETプローブが投与された画像が紹介された．この栄誉に浴したのはUCLA Barrioらのチーム，プローブは[^{18}F]FDDNP[5]であった．しかし[^{18}F]FDDNPは非特異的結合があまりにも多く，このプローブがスタンダードなAD診断用プローブになるとは考えにくい．

現時点で最も臨床試験実施例の多いプローブは，ピッツバーグ大Klunkらによって開発されたその数100例を超えると思われる[^{11}C]PIB[6]である．[^{11}C]PIBの最も優れた特徴は脳からのウォッシュアウトに優れていることであり，この特性に基づくと思われる非特異的結合が少ないことである．

[^{11}C]SB-13[7]はペンシルベニア大Kung夫妻らによって開発されたプローブであるが，ヒト画像はほとんど[^{11}C]PIBと同様といわれている．

著者らによって開発された[^{11}C]BF-227[8]のAD患者脳における集積像は，Aβないしは老人斑の空間的分布とほぼ一致するのが特徴である．

現在，世界中で主として研究用に使用されているアミロイドイメージング用PETプローブのほとんどは[^{11}C]標識体である．[^{11}C]標識プローブはその半減期の短さ(約20分)から，これを使用するためにはPET施設の極近隣にサイクロトロンおよび合成装置の併設が必要である．一方，もう一つの代表的PET用標識体である[^{18}F]はその半減期(約110分)が長く，サイクロトロンおよび合成装置を備えた製造拠点で標識合成し，PET施設へのデリバリーが可能であることなどから，診断用(臨床用)プローブとしての有用性は[^{11}C]のそれに比し圧倒的に優れている．これらのことから，次世代のアミロイドイメージング用プローブとして[^{18}F]標識体の開発が進行中であり，著者らもこれに取り組んでいる．

2007年6月末までに探索的臨床研究が実施されている[^{18}F]標識プローブはピッツバーグ大・General Electrics社の[^{18}F]PIB[9]，ペンシルベニア大(Avid社)・Bayer(Schering)社の[^{18}F]AV1/ZK[10]である．両プローブとも今後臨床例数が積み重ねられた後，プローブごとの評価が下されるであろう．また，開発者に巨大企業名がみられることからも，AD診断用の[^{18}F]標識プローブがいよいよ巨大ビジネスとして動きだすであろう未来をうかがわせる．

3. その他のアミロイドイメージング用プローブ

ADの病理像を追跡することにより同病を診断しようとするPETプローブ・PETを用いたアミロイドイメージングは，これまでのあらゆる診断法に比し，感度，特異度，診断精度などのいずれをとっても明らかに優れていることは確かである．しかしこの診断法には，将来的にみてもどうしても克服できないと予想される一つの課題がある．それは診断装置，すなわちPETの普及台数の問題である．今後，標識プロ

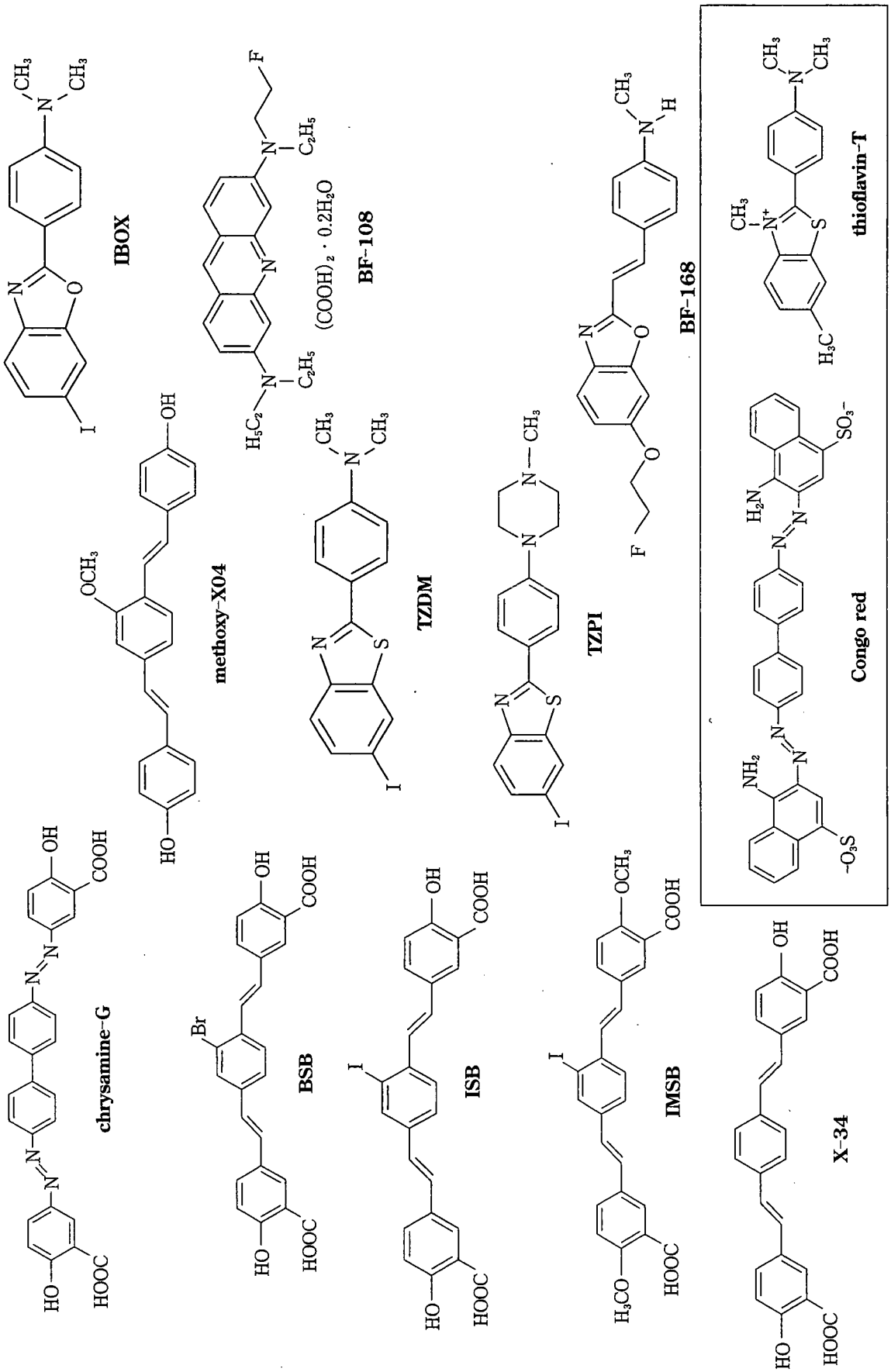

図1 アミロイドイメージング用に開発されたPETプローブ群

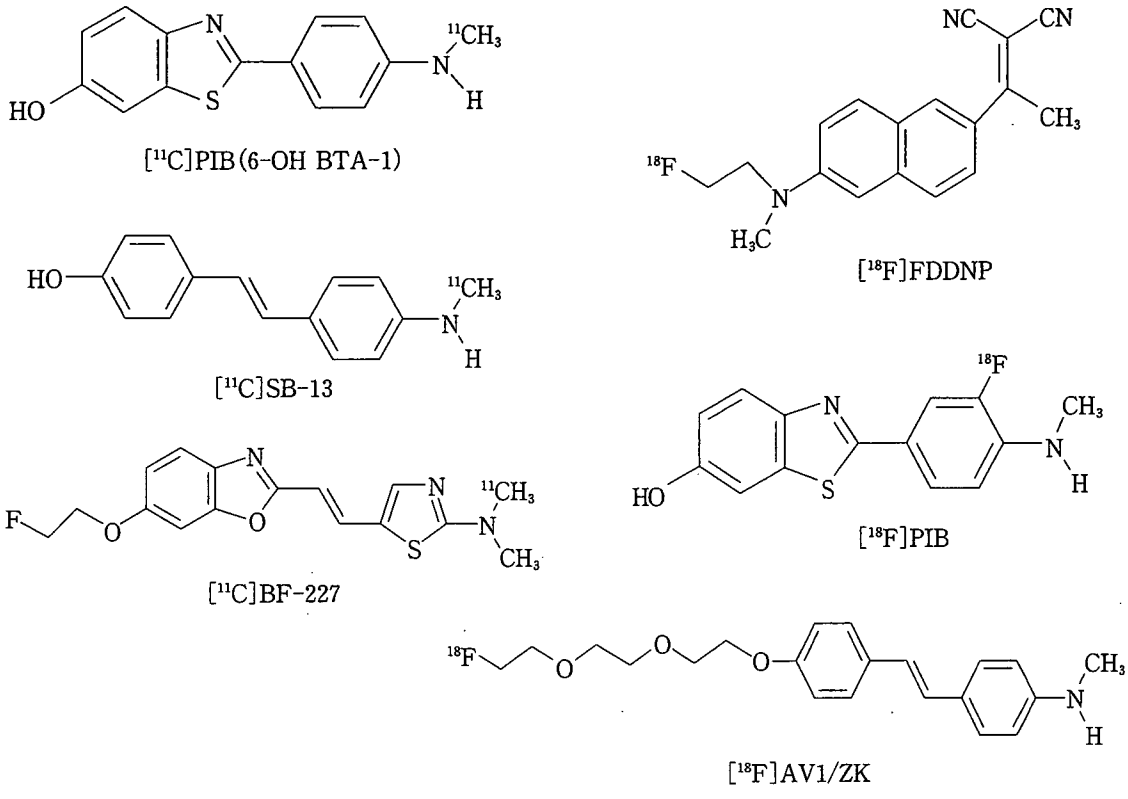

図2 臨床試験に供されたアミロイドイメージング用PETプローブ

ーブのデリバリーが日常化されたとしても，MRIやSPECTのように国内設置台数が数千といった普及は，PETにおいては到底到達不可能であろう．

そこでMRIまたはSPECTにそれぞれ対応したプローブを用いたアミロイドイメージングが試みられつつある．MRI用プローブについては，本誌樋口らの別稿を参照していただきたい．

次にSPECT用プローブであるが，ペンシルベニア大Kungらによって開発された[123I]IMPY[11]（**図3**）は，AD患者においてAβが蓄積することが知られている部位においてuptakeが増加していることが第10回国際アルツハイマー病学会にて報告された[11]．また，KungらはIMPY後も精力的にSPECT用プローブ候補化合物を報告している．一方，国内においてもSPECT用プローブの開発を進めている企業が存在することを聞いている．

最近，より簡便なAD診断法として近赤外線蛍光(near infra-red fluorescence: NIRF)プローブ・蛍光イメージング診断装置が注目されている．その診断原理はAβに親和性をもち，しかも血液-脳関門を越え，更に生体を透過する光(波長約600-1,000nm，いわゆる生体の分光学的窓領域)を照射することによって同領域波長の蛍光を発するNIRFプローブをAD診断に応用しようとするものである．

この診断に用いる蛍光イメージング診断装置はベッドサイド，外来を問わず可搬性に優れており，放射線を利用せず，また，短時間での診断，集団検診または人間ドックへの応用が可能である．

この診断に用いるプローブについては最初のプロトタイププローブAOI-987[12]，更にNIAD-4[13]（いずれも**図3**）も既に紹介されており，著者らもその開発に取り組んでいる．

図4は著者らが見いだしたAβに親和性を有するNIRFプローブを，脳内にAβが蓄積するTgおよび野生型マウスに静脈内投与し，小動物用NIRFイメージング装置で撮影した例であるが，Tgマウス脳においてAβとプローブとの結合が示唆される画像が観察された．

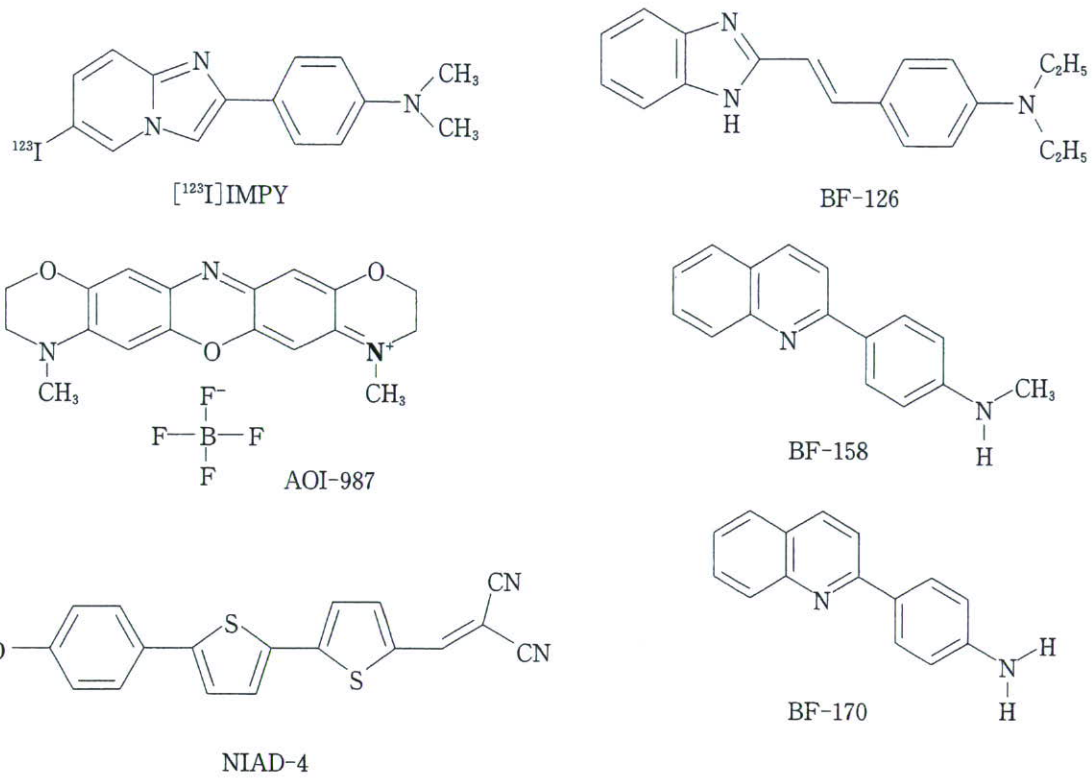

図3 アミロイドイメージング用に開発されたSPECTプローブ(IMPY)および近赤外線蛍光(NIRF)プローブ(AOI-987, NIAD-4), ならびにタウイメージング用に開発されたプローブ(BF-126, BF-158, BF-170)

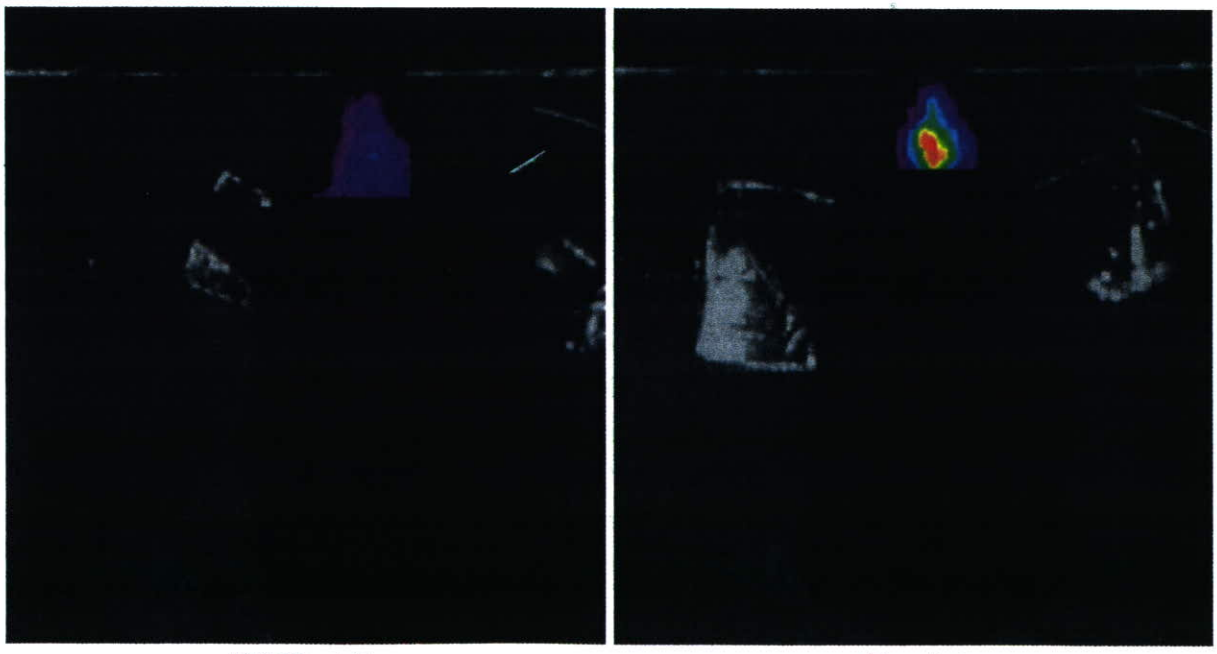

野生型マウス　　Tgマウス

図4 TgマウスにAβ親和性近赤外線蛍光(NIRF)プローブを投与した際の蛍光イメージング

著者らが見いだしたNIRFプローブをAβ脳内蓄積Tgおよび野生型マウスに静脈内投与し, 小動物用NIRFイメージング装置で撮影した. Tgマウス脳においてAβとプローブとの結合が示唆される画像が観察された. (提供:GEヘルスケアバイオサイエンス株式会社)

AD診断用NIRFプローブ開発の難しさは，従来のアミロイドイメージング用プローブの備えるべき特性に加えて，波長，量子収率，ストークスシフトなど，多くの克服すべき課題が存在することである．更に現状の蛍光イメージング装置は小動物用においてでさえも必ずしもプローブ開発者を満足させるレベルにはなく，プローブとともに診断装置の更なる進化も必要であることを痛感している．

しかし，将来のAD診断はその簡便さからNIRFプローブ・蛍光イメージング診断装置で最初のスクリーニングが行われ，疑わしい場合はPETプローブ・PETで診断という2段階になる可能性が高いと著者らは推測している．

4. タウイメージング用PETプローブ

AD患者脳内において特有の病理像を示す蛋白，すなわちAβ（ないしは老人斑）と（過剰リン酸化）タウ蛋白（ないしは神経原線維変化）の両者はβシート構造をとるが，これまでAβを認識する，あるいはAβとタウ蛋白の両者を認識するプローブは数多く報告されているが，選択的にタウ蛋白を認識するプローブは著者らが見いだした化合物群（BF-126，BF-158，BF-170）[14]のみである（図3）．

タウイメージングはADの進行度ないしは重症度診断にはむしろアミロイドイメージングに勝る有用性を示すと予想されてはいるが，臨床試験に供されたタウイメージング用PETプローブはいまだ報告されていない．

謝辞 著者らの研究には科学技術振興調整費，独立行政法人医薬基盤研究所の‘保健医療分野における基礎研究推進事業’，厚生労働科学研究費補助金の‘基礎研究成果の臨床応用推進研究事業’，同‘長寿科学総合研究事業’，同‘難治性疾患克服事業’，新エネルギー・産業技術総合開発機構（NEDO）産業技術研究助成事業の支援をいただきました．またBF研究所に出資していただきました医薬品医療機器総合機構および各社に感謝いたします．本研究には‘平成16年度三井住友海上福祉財団研究助成金’，‘ノバルティス老化および老年医学研究基金’，‘アストラゼネカ・リサーチグラント’の支援をいただきました．最後に共同研究者の福祉村病院 長寿医学研究所 赤津裕康，山本孝之，東北大学医学部 老年/漢方内科 荒井啓行，同機能薬理学分野 谷内一彦諸先生，旧BF研究所アミロイドイメージング研究チームおよび現東北大学PETイメージング研究チームの同僚に感謝の意を表します．

文 献

1) Zhuang ZP, et al: Radioiodinated styrylbenzenes and thioflavins as probes for amyloid aggregates. J Med Chem **44**: 1905-1914, 2001.
2) Lockhart A, et al: Evidence for the presence of three distinct binding sites for the thioflavin T class of Alzheimer's disease PET imaging agents on beta-amyloid peptide fibrils. J Biol Chem **280**: 7677-7684, 2005.
3) Tipre DN, et al: PET imaging of brain 5-HT1A receptors in rat in vivo with ^{18}F-FCWAY and improvement by successful inhibition of radioligand defluorination with miconazole. J Nucl Med **47**: 345-353, 2006.
4) Klunk WE, et al: Development of small molecule probes for the beta-amyloid protein of Alzheimer's disease. Neurobiol Aging **15**: 691-698, 1994.
5) Shoghi-Jadid K, et al: Localization of neurofibrillary tangles and beta-amyloid plaques in the brains of living patients with Alzheimer disease. Am J Geriatr Psychiatry **10**: 24-35, 2002.
6) Klunk WE, et al: Imaging brain amyloid in Alzheimer's disease with Pittsburgh Compound-B. Ann Neurol **55**: 306-319, 2004.
7) Verhoeff NP, et al: In-vivo imaging of Alzheimer disease beta-amyloid with [^{11}C]SB-13 PET. Am J Geriatr Psychiatry **12**: 584-595, 2004.
8) Kudo Y, et al: 2-(2-[2-Dimethylaminothiazol-5-yl]ethenyl)-6-(2-[fluoro]ethoxy) benzoxazole: a novel PET agent for in vivo detection of dense amyloid plaques in Alzheimer's disease patients. J Nucl Med **48**: 553-561, 2007.
9) Mathis CA, et al: Comparison of the amyloid imaging agents [F-18]3'-F-PIB and [C-11]PIB in

Alzheimer's disease and control subjects. J Nucl Med 48(Suppl 2): 56, 2007.
10) Rowe CC, et al: First results from human studies of a novel F-18 PET ligand for brain β-amyloid imaging. J Nucl Med 48(Suppl 2): 57, 2007.
11) Clark CM, et al: Imaging amyloid with I^{123}IMPY SPECT. Alzheimer's & Dementia 2(Suppl 2): 342, 2006.
12) Hintersteiner M, et al: In vivo detection of amyloid-beta deposits by near-infrared imaging using an oxazine-derivative probe. Nat Biotechnol 23: 577-583, 2005.
13) Nesterov EE, et al: In vivo optical imaging of amyloid aggregates in brain: design of fluorescent markers. Angew Chem Int Ed Engl 44: 5452-5456, 2005.
14) Okamura N, et al: Quinoline and benzimidazole derivatives: candidate probes for in vivo imaging of tau pathology in Alzheimer's disease. J Neurosci 25: 10857-10862, 2005.